Entangling Macroscopic Diamonds at Room Temperature

K. C. Lee, *et al.*

Science **334**, 1253 (2011);
DOI: 10.1126/science.1211914

This copy is for your personal, non-commercial use only.

If you wish to distribute this article to others, you can order high-quality copies for your colleagues, clients, or customers by clicking here.

Permission to republish or repurpose articles or portions of articles can be obtained by following the guidelines here.

The following resources related to this article are available online at www.sciencemag.org (this infomation is current as of December 2, 2011):

Updated information and services, including high-resolution figures, can be found in the online version of this article at:
http://www.sciencemag.org/content/334/6060/1253.full.html

Supporting Online Material can be found at:
http://www.sciencemag.org/content/suppl/2011/11/30/334.6060.1253.DC1.html

This article **cites 31 articles**, 2 of which can be accessed free:
http://www.sciencemag.org/content/334/6060/1253.full.html#ref-list-1

This article has been **cited by** 1 articles hosted by HighWire Press; see:
http://www.sciencemag.org/content/334/6060/1253.full.html#related-urls

This article appears in the following **subject collections:**
Physics
http://www.sciencemag.org/cgi/collection/physics

Science (print ISSN 0036-8075; online ISSN 1095-9203) is published weekly, except the last week in December, by the American Association for the Advancement of Science, 1200 New York Avenue NW, Washington, DC 20005. Copyright 2011 by the American Association for the Advancement of Science; all rights reserved. The title *Science* is a registered trademark of AAAS.

4. N. Yoshida, K. Omukai, L. Hernquist, T. Abel, *Astrophys. J.* **652**, 6 (2006).
5. B. W. O'Shea, M. L. Norman, *Astrophys. J.* **654**, 66 (2007).
6. N. Yoshida, K. Omukai, L. Hernquist, *Science* **321**, 669 (2008).
7. H. W. Yorke, P. Bodenheimer, *Astrophys. J.* **525**, 330 (1999).
8. C. F. McKee, J. C. Tan, *Astrophys. J.* **681**, 771 (2008).
9. H. W. Yorke, A. Welz, *Astron. Astrophys.* **315**, 555 (1996).
10. H. W. Yorke, C. Sonnhalter, *Astrophys. J.* **569**, 846 (2002).
11. K. Omukai, F. Palla, *Astrophys. J.* **589**, 677 (2003).
12. T. Hosokawa, K. Omukai, *Astrophys. J.* **691**, 823 (2009).
13. This definition of accretion luminosity includes the mechanical luminosity of an accretion-driven wind, and the ratio $t_{\mathrm{KH}}/t_{\mathrm{acc}}$ is equal to the ratio L_{acc}/L_*.
14. D. Ezer, A. G. W. Cameron, *Astrophys. Space Sci.* **14**, 399 (1971).
15. D. Schaerer, *Astron. Astrophys.* **382**, 28 (2002).
16. H. Umeda, K. Nomoto, *Astrophys. J.* **565**, 385 (2002).
17. A. Heger, S. E. Woosley, *Astrophys. J.* **567**, 532 (2002).
18. J. Tumlinson, A. Venkatesan, J. M. Shull, *Astrophys. J.* **612**, 602 (2004).
19. A. Frebel, J. L. Johnson, V. Bromm, *Mon. Not. R. Astron. Soc.* **392**, L50 (2009).
20. N. Iwamoto, H. Umeda, N. Tominaga, K. Nomoto, K. Maeda, *Science* **309**, 451 (2005).
21. B. W. O'Shea, T. Abel, D. Whalen, M. L. Norman, *Astrophys. J.* **628**, L5 (2005).
22. N. Yoshida, K. Omukai, L. Hernquist, *Astrophys. J.* **667**, L117 (2007).
23. [Fe/H] ≡ $\log(\mathrm{Fe/H})_{\mathrm{star}} - \log(\mathrm{Fe/H})_{\mathrm{sun}}$, where (Fe/H) is mass ratio of Fe to H.
24. T. Hosokawa, K. Omukai, *Astrophys. J.* **703**, 1810 (2009).
25. E. Caffau *et al.*, *Nature* **477**, 67 (2011).
26. T. Ohkubo, K. Nomoto, H. Umeda, N. Yoshida, S. Tsuruta, *Astrophys. J.* **706**, 1184 (2009).
27. M. J. Turk, T. Abel, B. O'Shea, *Science* **325**, 601 (2009).
28. P. C. Clark *et al.*, *Science* **331**, 1040 (2011).
29. G. Chabrier, *Publ. Astron. Soc. Pac.* **115**, 763 (2003).

Acknowledgments: We thank T. Nakamura, K. Nomoto, S. Inutsuka, and N. Turner for stimulating discussions on this topic. Comments by an anonymous referee helped improve the manuscript. T.H. appreciates the support by Fellowship of the Japan Society for the Promotion of Science for Research Abroad. The present work is supported in part by the grants-in-aid by the Ministry of Education, Science and Culture of Japan (19047004, 2168407, 21244021:KO, 20674003:NY). Portions of this research were conducted at the Jet Propulsion Laboratory, California Institute of Technology, which is supported by NASA. Data analysis was (in part) carried out on the general-purpose PC farm at Center for Computational Astrophysics (CfCA) of National Astronomical Observatory of Japan.

Supporting Online Material

www.sciencemag.org/cgi/content/full/science.1207433/DC1
Materials and Methods
SOM Text
Figs. S1 to S7
Tables S1 and S2
References (*30–64*)

25 April 2011; accepted 28 October 2011
Published online 10 November 2011;
10.1126/science.1207433

Entangling Macroscopic Diamonds at Room Temperature

K. C. Lee,[1]* M. R. Sprague,[1]* B. J. Sussman,[2] J. Nunn,[1] N. K. Langford,[1] X.-M. Jin,[1,3] T. Champion,[1] P. Michelberger,[1] K. F. Reim,[1] D. England,[1] D. Jaksch,[1,3] I. A. Walmsley[1]†

Quantum entanglement in the motion of macroscopic solid bodies has implications both for quantum technologies and foundational studies of the boundary between the quantum and classical worlds. Entanglement is usually fragile in room-temperature solids, owing to strong interactions both internally and with the noisy environment. We generated motional entanglement between vibrational states of two spatially separated, millimeter-sized diamonds at room temperature. By measuring strong nonclassical correlations between Raman-scattered photons, we showed that the quantum state of the diamonds has positive concurrence with 98% probability. Our results show that entanglement can persist in the classical context of moving macroscopic solids in ambient conditions.

Our intuition about the nature of the physical world is strongly conditioned by the experience that macroscopic solids move according to the rules of classical mechanics. Quantum theory, however, asserts that superpositions and entanglement are possible even for large objects. Therefore, exploration of the persistence of quantum correlations in the traditionally classical realm is important for both fundamental science and technology, because of the implications for physics beyond conventional quantum mechanics (*1*) and for quantum information processing, which requires sustained coherence across many particles (*2*).

The two main barriers for creating superpositions and entanglement in the mechanical motion of macroscopic systems are strong internal interactions, which complicate the dynamics, and strong coupling with the environment, which leads to short decoherence times. The standard approach is to design systems with well-defined and long-lived normal modes that can be selectively excited, and then to cool them to remove thermal noise and isolate them from the environment. Substantial progress has been made toward demonstrating strong quantum signatures in larger systems—for example, in optomechanical (*3*–*5*), molecular (*6*), and superconducting (*7*) systems. Mechanical oscillators can now be cooled to the thermal ground state (*7*–*9*).

A different approach is required, however, to reveal quantum features in the motion of "ordinary" solids in the high-entropy environment present at ambient conditions. Without a specially engineered system, measurements must be made on time scales shorter than the characteristically fast coherence decay times of a real-world system. This can be achieved with ultrashort optical pulses. Recent studies of quantum coherence in biology have used ultrafast probes and interference measurements to establish the persistence of quantum behavior in naturally occurring bulk systems (*10*, *11*). To probe entanglement, however, it is also necessary to access the correlations of the excited modes.

We study excitations of the optical phonon mode in diamond, a bulk vibration consisting of two counter-oscillating sublattices within the diamond structure. The optical phonons are macroscopic, persistent excitations distributed over ~10^{16} atoms within the crystals. The phonons have a very high carrier frequency of 40 THz owing to the extremely strong interactions between neighboring atoms, giving rise to a mechanically stiff lattice. This large energy, compatible with the ultrashort pulses in our experiment (bandwidth ~7 THz), also eliminates the need for cooling or optical pumping, because thermal excitations are negligible at room temperature. The specific experimental protocol that we use is based on the well-known DLCZ scheme (*12*) and previous pioneering experiments in cold atomic ensembles (*13*–*16*). We first create a phonon via spontaneous Raman scattering from a strong optical pump pulse, an event that is simultaneously accompanied by the emission of a Stokes photon (red-shifted from the pump). After this interaction, the joint state of the diamond and the Stokes mode can be written as

$$|\psi_s\rangle \approx \left[1 + \varepsilon_s s^\dagger(t_s) b^\dagger(t_s)\right] |\mathrm{vac}\rangle \qquad (1)$$

where $|\varepsilon_s|^2 << 1$ is the scattering probability and $|\mathrm{vac}\rangle = |\mathrm{vac}_{\mathrm{opt}}\rangle \otimes |\mathrm{vac}_{\mathrm{vib}}\rangle$ is the joint optical and vibrational vacuum state containing no photons and no phonons; s and b are the bosonic annihilation operators for the Stokes and phonon modes, respectively, evaluated at the time t_s when the pump pulse exits the diamond. Equation 1 describes an entangled state of optical and material modes, which is already nonclassical. To entangle two diamonds, we simultaneously pump two separate crystals—producing the state $|\Psi_s\rangle = |\psi_{sL}\rangle|\psi_{sR}\rangle$, where L and R denote the left and right diamonds, respectively—and we combine their Stokes modes on a polarizing beamsplitter (Fig. 1). The Stokes modes are caused to interfere with relative phase φ_s by means of a half-wave plate and polarizer. Detection of a Stokes photon at a detector D_s placed behind the polarizer corresponds to application of the measurement (*17*) $E = \langle \mathrm{vac}_{\mathrm{opt}}|s(t'_s)$, where t'_s is

---

[1] Clarendon Laboratory, University of Oxford, Parks Road, Oxford OX1 3PU, UK. [2] National Research Council of Canada, Ottawa, Ontario K1A 0R6, Canada. [3] Centre for Quantum Technologies, National University of Singapore, Singapore.

*These authors contributed equally to this work.

†To whom correspondence should be addressed. E-mail: walmsley@physics.ox.ac.uk

the time at which the Stokes photon strikes D_s. Tracking the evolution of the Stokes operator through the optical setup $s(t'_s) = s_L(t_s) + e^{i\varphi_s}s_R(t_s)$ [neglecting normalization and global phases; see (*18*)], we obtain the state

$$E|\psi_s\rangle = [b_L^\dagger(t_s) + e^{-i\varphi_s}b_R^\dagger(t_s)]|\text{vac}_\text{vib}\rangle \quad (2)$$

which is an entangled state of the two diamonds at t_s containing a single phonon excitation distributed across the two crystals.

Observing a Stokes-scattered photon at D_s therefore allows us to infer the presence of entanglement between the diamonds. We then test this inference by directing strong probe pulses into the crystals at a time $T = 350$ fs after t_s, which is short compared to the coherence lifetime of 7 ps (*19*). Unlike similar experiments with atomic ensembles, the diamonds must be probed before the Stokes photon has reached D_s (*18*). The conventional time ordering could be recovered with the use of a chip-scale interferometer (*20*) and fast detectors (*21*). With small probability $|\varepsilon_a|^2 << 1$ the phonon is converted into a 40-THz blue-shifted anti-Stokes photon, $b \rightarrow b + \varepsilon_a a$, so that the joint state of the diamonds and anti-Stokes modes is

$$|\psi_a\rangle = \{b_L^\dagger(t_a) + e^{-i\varphi_s}b_R^\dagger(t_a) + \varepsilon_a[a_L^\dagger(t_a) + e^{-i\varphi_s}a_R^\dagger(t_a)]\}|\text{vac}\rangle \quad (3)$$

where a is the annihilation operator for an anti-Stokes photon, and $t_a = t_s + T$. The anti-Stokes modes are combined on a polarizing beamsplitter, and interfered, with a controllable phase φ_a, by means of a half-wave plate and another polarizing beamsplitter. The numbers of anti-Stokes photons, $N_\pm$, that are detected emerging from the two output ports are given by $|\langle\text{vac}|a_\pm(t_a')|\Psi_a\rangle|^2 \propto \varepsilon_a^2\sin^2[(\varphi_a + \varphi_s + \pi \pm \pi)/2]$, where $a_\pm(t_a') = [a_L(t_a) \pm e^{i\varphi_a}a_R(t_a)]/\sqrt{2}$ and t_a' is the time at which anti-Stokes photons are detected. We use the copropagating pump and probe fields to actively stabilize φ_s and φ_a separately, so that the entanglement generation and verification

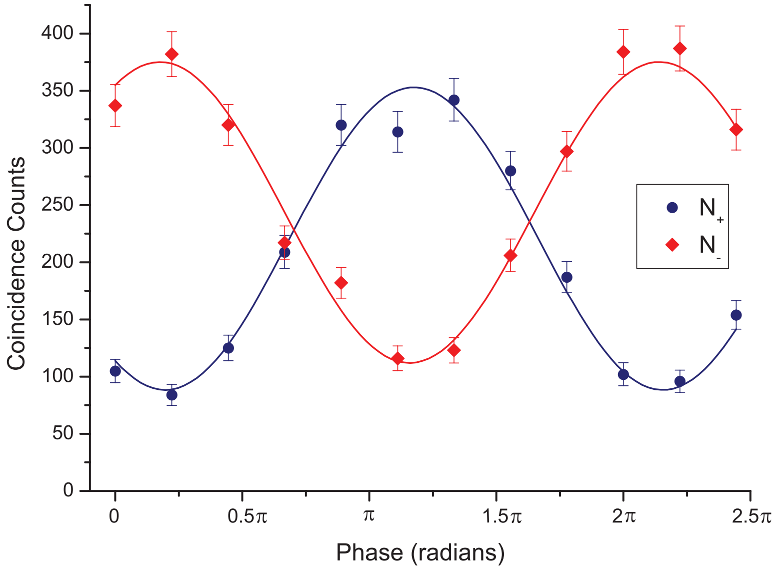

Fig. 2. Coincidence between herald and readout photons. The visibility is $V = (61 \pm 3)\%$ for N_+ and $V = (55 \pm 3)\%$ for N_-. The difference in visibility between the measurement sets we attribute to the different rate of accidental coincidences between the two detectors. Error bars on the plot are estimated from the standard deviation of a Poissonian process.

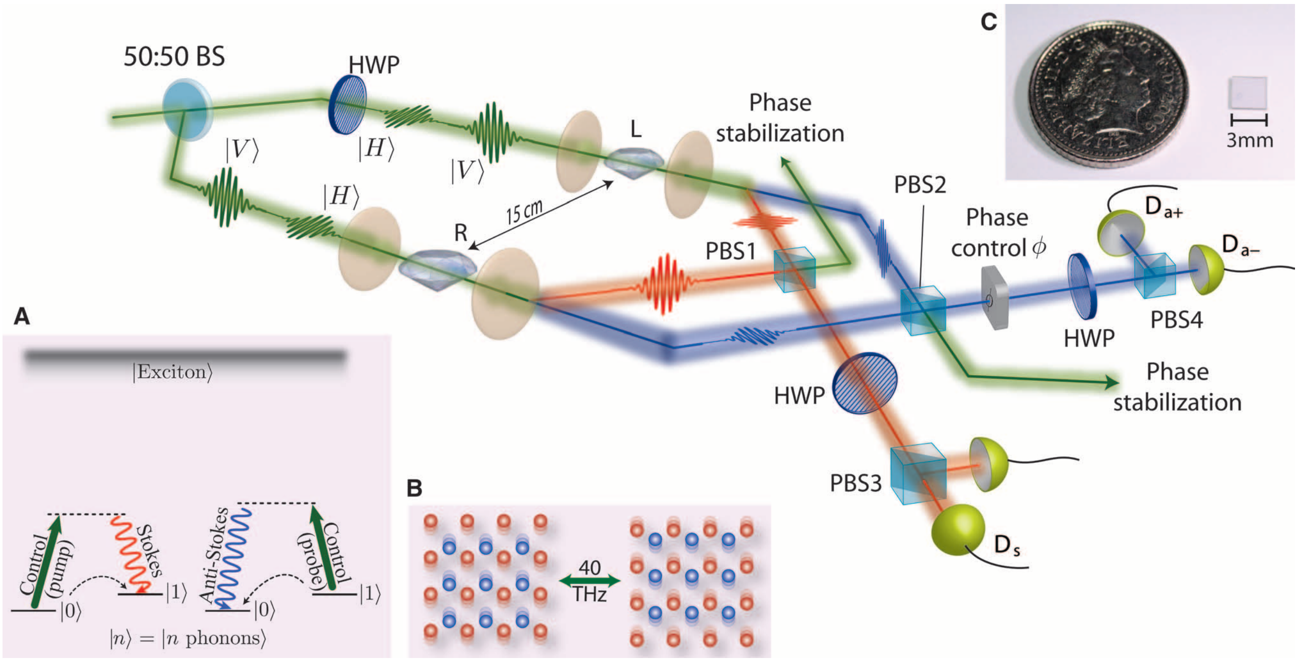

Fig. 1. Schematic of the experimental layout for generating entanglement between two diamonds. A pump pulse is split by the beamsplitter BS and focused onto two spatially separated diamonds. Optical phonons are created by spontaneous Raman scattering, generating the orthogonally polarized heralding Stokes fields s_L, s_R [see inset (**A**): $|n\rangle$ represents phonon number states in diamond]. Polarization beamsplitter PBS1 combines the spatial paths, and the half-wave plate HWP rotates and mixes the fields on PBS3, which are then directed into the single-photon detector D_s. A probe pulse, with programmable delay, coherently maps the optical phonon into the orthogonally polarized anti-Stokes fields a_L, a_R [see inset (A)], which are similarly combined and mixed on PBS2 and PBS4, and detected on the detectors D_{a+}, D_{a-}. The relative phase φ_a between the fields $a_{L,R}$ is controlled by a sequence of quarter- and half-wave plates (*18*). Rejected pump beams from PBS1,2 are used to stabilize the interferometer. Displacements of neighboring atoms from their equilibrium positions are anticorrelated in the optical phonon mode [see inset (**B**)], with a vibrational period of 25 fs in diamond. Inset (**C**) shows one of the diamond samples, with a coin for scale.

processes are independent (*22*). The sinusoidal oscillations of $N_\pm$ with the phase φ_a, indicating that the coherence between the two diamond modes has been preserved, are plotted in Fig. 2 for the Stokes detector D_s.

The fringe visibility is $V = (61 \pm 3)\%$ (for N_+), which, when compared to the theoretical maximum of ~75% (*18*) for a two-mode squeezed state, implies that we have two well-defined modes, with good mode overlap between the Raman-scattered modes interfered from the two diamonds. Causes of decorrelation include spontaneous emission of anti-Stokes photons (*18*) and decoherence of the phonon, as well as limited coupling efficiency due to scattering into higher-order spatial modes, indicating that our measurement represents a lower bound on the intrinsic correlation between the phonons.

To verify entanglement between the two phonon modes of the diamonds, we examine the entanglement between the Stokes and anti-Stokes photons (here we consider only N_+ from Fig. 2). Because the phonon-to-photon mapping is a local operation (acting separately on each diamond) that cannot increase entanglement (*16*), the photon entanglement is a strict lower bound to the phonon entanglement. Therefore, considering the photon modes, we must show that the probability of generating higher-order terms is inconsistent with any separable state (e.g., of the form $|\Psi_a\rangle = (1 + \varepsilon_a a_L^\dagger)(1 + \varepsilon_a a_R^\dagger)|\mathrm{vac}\rangle$). That is, the probability of twin anti-Stokes readout detection events ($a_L^\dagger a_R^\dagger|\,\mathrm{vac}\rangle$) must be shown to be sufficiently small compared to the single anti-Stokes detection probability.

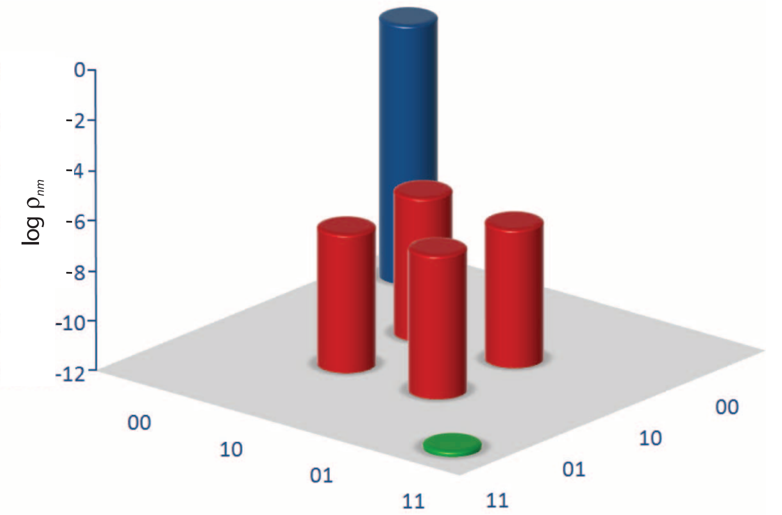

Fig. 3. Density matrix of the heralded anti-Stokes modes. The density matrix elements are $p_{00} = 1 - 2.3 \times 10^{-5}$, $p_{01} = 1.2 \times 10^{-5}$, $p_{10} = 1.1 \times 10^{-5}$, $d = 7.0 \pm 0.3 \times 10^{-6}$, $p_{11} = 2.0 \pm 1.1 \times 10^{-11}$. The diagonal element probabilities are maximum likelihood estimates, measured with no interference between the anti-Stokes modes of the two diamonds. No corrections for background counts, accidental coincidences, or system inefficiencies were made in these measurements.. The higher-order term is inherent to the process of spontaneous emission, and the vacuum component is related to the anti-Stokes readout, collection, and detector efficiencies.

To formalize this argument, we evaluate the concurrence (*23*), which is a monotonic measure of two-qubit entanglement that is zero for any separable state and positive for all entangled states. Here the concurrence is defined over a subspace that consists of detecting zero or one anti-Stokes photon at the two detectors heralded on the detection of a Stokes photon. We assume that the density matrix ρ describing the joint state of the anti-Stokes modes has the form shown in Fig. 3. The indices [0,1] indicate the number of photons detected in the anti-Stokes mode generated from diamond [L,R], conditioned on detecting a Stokes photon with detector D_s. The off-diagonal coherence d between $a_L^\dagger|\mathrm{vac}\rangle$ and $a_R^\dagger|\mathrm{vac}\rangle$ is estimated to be $d = V(p_{01} + p_{10})/2$, and all other terms are set to zero. This makes our estimate of the amount of entanglement conservative, as nonzero elements can only increase the concurrence (*16*). Higher-order photon number contributions are neglected. With these assumptions, the concurrence provides a strict lower bound to the entanglement between the diamonds (*16*).

The concurrence of ρ is therefore (*16*, *23*)

$$C = 2\ \max(|d| - \sqrt{p_{00}p_{11}}, 0) \qquad (4)$$

We estimate the concurrence to be $(5.2 \pm 2.6) \times 10^{-6}$, which is on the order of the maximum value of the concurrence (for $V = 1$, and $p_{11} = 0$ we have $C_{\max} = p_{01} + p_{10} = 2.3 \times 10^{-5}$). The maximum value is limited by coupling and detector efficiencies and the readout probability (the probability of converting a phonon into an anti-Stokes photon, conditioned on detecting a Stokes photon).

To determine our confidence in concluding that the system is entangled, we calculate the Poissonian confidence level (*24*) for positive concurrence when we detect X twin readout events

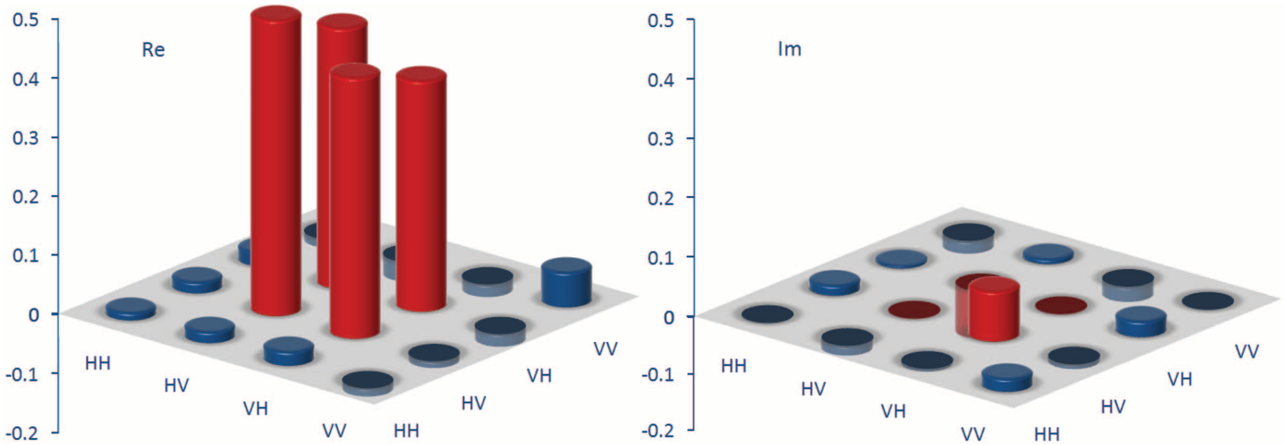

Fig. 4. Reconstructed real (Re) and imaginary (Im) components of the joint polarization state of the Stokes and anti-Stokes modes, projected into the subspace containing one photon in each mode. HV, for example, indicates a horizontally polarized Stokes photon and vertically polarized anti-Stokes photon, where polarization is used to encode the time ordering of pulses [see SOM (*18*)] The state appears to be highly entangled in polarization after postselection of this subspace, which demonstrates strong coherence between the diamonds, suggestive of near-maximal entanglement. This complements the evidence for genuine entanglement provided by Fig. 3.

$(a_L^\dagger a_R^\dagger|\text{vac}\rangle)$ given an expected mean number of events $\mu_0 = d^2 N p_s$ consistent with zero concurrence, where $p_s = 1.0 \times 10^{-3}$ is the probability of generating a Stokes heralding photon and N is the number of experimental runs. Our results ($X = 3$, $N = 1.9 \times 10^{14}$, and $\mu_0 = 9.1 \pm 0.9$) indicate positive concurrence at a 98 ± 1% confidence level. Therefore, based on this detection of entanglement between Stokes and anti-Stokes modes, we can infer entanglement between the phonon modes of two macroscopic solids at room temperature.

Finally, we examine the quality of entanglement generated between the diamonds by neglecting the vacuum component in Fig. 3, which is only caused by inefficiencies in coupling, detection, and readout of the anti-Stokes mode. To do this, we performed quantum state tomography (*25*) on the joint polarization state of the Stokes and anti-Stokes modes, postselecting on the detection of both photons. The reconstructed state is shown in Fig. 4, and we have subtracted accidental coincidences calculated from the Stokes and anti-Stokes singles rates. These results provide a more complete estimate of the coherence between the two modes than the interference fringes in Fig. 2. The concurrence of this subspace, 0.85, provides an estimate of the achievable entanglement between the two diamond phonon modes as the readout efficiency, coupling, and detector efficiencies approach unity (i.e., $p_{00} \to 0$). Further, the fidelity to the nearest Bell state $[|HV\rangle + |VH\rangle]/\sqrt{2}$ is 0.91. However, in the presence of real coupling and detection losses, the existence of entanglement can only be inferred from the density matrix in Fig. 3 (*22*).

In our experiment, short-lived quantum correlations were revealed by combining an ultrafast interferometric pump-probe scheme with photon-counting techniques. The large optical bandwidth enabled the resolution of extremely fast dynamics in the solids, and also operation at high data rates, providing sufficient statistics to establish entanglement even in the presence of losses. This approach lays the foundation for future studies of quantum phenomena in many-body, strongly interacting systems coupled to strongly decohering environments and points toward a novel platform for ultrafast quantum information processing at room temperature.

References and Notes

1. R. Penrose, in *Mathematical Physics*, A. Fokas, T. W. B. Kibble, A. Grigoriou, B. Zegarlinski, Eds. (Imperial College Press, London, 2000), pp. 266–282.
2. D. P. DiVincenzo, *Fortschr. Phys.* **48**, 771 (2000).
3. S. Gigan *et al*., *Nature* **444**, 67 (2006).
4. J. D. Thompson *et al*., *Nature* **452**, 900 (2008).
5. B. Abbott *et al*., *New J. Phys.* **11**, 073032 (2009).
6. S. Gerlich *et al*., *Nat Commun* **2**, 263 (2011).
7. A. D. O'Connell *et al*., *Nature* **464**, 697 (2010).
8. J. D. Teufel *et al*., *Nature* **475**, 359 (2011).
9. J. Chan *et al*., *Nature* **478**, 89 (2011).
10. G. Panitchayangkoon *et al*., *Proc. Natl. Acad. Sci. U.S.A.* **107**, 12766 (2010).
11. E. Collini *et al*., *Nature* **463**, 644 (2010).
12. L.-M. Duan, M. D. Lukin, J. I. Cirac, P. Zoller, *Nature* **414**, 413 (2001).
13. T. Chanelière *et al*., *Nature* **438**, 833 (2005).
14. K. S. Choi, H. Deng, J. Laurat, H. J. Kimble, *Nature* **452**, 67 (2008).
15. D. N. Matsukevich, A. Kuzmich, *Science* **306**, 663 (2004).
16. C. W. Chou *et al*., *Nature* **438**, 828 (2005).
17. G. Milburn, *J. Opt. Soc. Am. B* **24**, 167 (2007).
18. See supplementary information on *Science* Online.
19. K. C. Lee *et al*., *Diam. Relat. Mater.* **19**, 1289 (2010).
20. A. Greentree, B. Fairchild, F. Hossain, S. Prawer, *Mater. Today* **11**, 22 (2008).
21. L. Prechtel *et al*., *Nano Lett.* **11**, 269 (2011).
22. S. J. van Enk, *Phys. Rev. A* **75**, 052318 (2007).
23. W. Wootters, *Phys. Rev. Lett.* **80**, 2245 (1998).
24. G. J. Feldman, R. D. Cousins, *Phys. Rev. D Part. Fields* **57**, 3873 (1998).
25. D. F. V. James, P. G. Kwiat, W. J. Munro, A. G. White, *Phys. Rev. A* **64**, 052312 (2001).

Acknowledgments: We thank V. Vedral, A. Datta, and L. Zhang for valuable insights. This work was supported by the Royal Society, Engineering and Physical Sciences Research Council (grant GR/S82176/01), EU IP Q-ESSENCE (grant 248095), EU ITN FASTQUAST, U.S. European Office of Aerospace Research and Development (grant 093020), Clarendon Fund, St. Edmund Hall, and Natural Sciences and Engineering Research Council of Canada.

Supporting Online Material
www.sciencemag.org/cgi/content/full/334/6060/1253/DC1
Materials and Methods
SOM Text
References (*26–36*)

29 July 2011; accepted 27 October 2011
10.1126/science.1211914

Enhancing Hydrogen Evolution Activity in Water Splitting by Tailoring Li^+-Ni(OH)_2-Pt Interfaces

Ram Subbaraman,[1,2] Dusan Tripkovic,[1] Dusan Strmcnik,[1] Kee-Chul Chang,[1] Masanobu Uchimura,[1,3] Arvydas P. Paulikas,[1] Vojislav Stamenkovic,[1] Nenad M. Markovic[1]*

Improving the sluggish kinetics for the electrochemical reduction of water to molecular hydrogen in alkaline environments is one key to reducing the high overpotentials and associated energy losses in water-alkali and chlor-alkali electrolyzers. We found that a controlled arrangement of nanometer-scale Ni(OH)_2 clusters on platinum electrode surfaces manifests a factor of 8 activity increase in catalyzing the hydrogen evolution reaction relative to state-of-the-art metal and metal-oxide catalysts. In a bifunctional effect, the edges of the Ni(OH)_2 clusters promoted the dissociation of water and the production of hydrogen intermediates that then adsorbed on the nearby Pt surfaces and recombined into molecular hydrogen. The generation of these hydrogen intermediates could be further enhanced via Li^+-induced destabilization of the HO–H bond, resulting in a factor of 10 total increase in activity.

Electrocatalysis of the hydrogen evolution reaction (HER) is critical to the operation of water-alkali electrolyzers (*1*–*6*), in which hydrogen is the main product, and chlor-alkali electrolyzers (*5*, *6*), in which it is a side product. These two technologies are highly energy-intensive and are known to account for ~25 to 30% (87,600 to 92,000 GWh/year) of the total electrical energy consumption by industrial processes in the United States (*3*, *7*). The HER is also an electrochemical reaction of fundamental scientific importance; the basic laws of electrode kinetics, as well as many modern concepts in electrocatalysis, were developed and verified by examining the reaction mechanisms related to the charge transfer–induced conversion of protons (in acid solutions) and water (in alkaline solutions) to molecular hydrogen.

Although previous studies have helped to rationalize which surface properties govern the variations in reactivity among catalysts (*8*–*12*), many key questions concerning the HER remain unanswered. For example, it is not clear why the rate of the HER is ~2 to 3 orders of magnitude lower at pH = 13 than at pH = 1, nor why the reaction is sensitive to the catalyst surface structure in alkaline media but largely insensitive in acids (*13*–*17*). A practical implication of the slow kinetics in alkaline solution is the lower energy efficiency for both water-alkali and chlor-alkali electrolyzers. For water-alkali electrolyzers, the high overpotentials for the oxygen evolution reaction (OER) at the anode also contribute significantly overall energy losses (*18*). This has led to various approaches to identify catalysts for both the OER and HER. However, such design strategies have rarely been based on molecular-level understanding of the reaction pathways. In addition, the influence of noncovalent (van der Waals–type) interactions on the overall kinetics of the HER has been underexplored, particularly in light of recent studies highlighting the impact of noncovalent interactions on the rates of many electrochemical reactions such as the oxygen reduction reaction, together with CO and methanol oxidation reactions (*19*–*22*).

Currently, various combinations of metals (Pt, Pd, Ir, Ru, Ag, Ni), metal alloys (Ni-Co, Ni-Mn, Ni-Mo), metal oxides (RuO_2), and Ni sulfides and phosphides are used to catalyze the conver-

---

[1] Materials Science Division, Argonne National Laboratory, Lemont, IL 60559, USA. [2] Nuclear Engineering Division, Argonne National Laboratory, Lemont, IL 60559, USA. [3] Advanced Materials Laboratory, Nissan Research Center, Kanagawa 237-8523, Japan.

*To whom correspondence should be addressed. E-mail: nmmarkovic@anl.gov